RPE | Radiation Physics & Engineering
An International Peer-Reviewed Journal
Published by K.N. Toosi University of Technology
http://rpe.kntu.ac.ir
Research Article

Radiation Physics and Engineering 2020; 1(4):55–64
https://doi.org/10.22034/RPE.2020.104842

Bohr Hamiltonian and interplay between γ-stable and γ-rigid collective motions with both Harmonic oscillation and Ring-shaped potentials for the γ-part

Nahid Soheibi[a], Mahdi Eshghi[b,*], Majid Hamzavi[c], Mohsen Bigdeli[a]

[a] *Department of Physics, University of Zanjan, Zanjan, Iran*
[b] *Department of Physics, Imam Hossein Comprehensive University, Tehran, Iran*
[c] *Department of Mathematics and Statistics, University of Texas at El Paso, El Paso, TX, USA*

HIGHLIGHTS

- The eigenvalue and eigenvector were obtained by the Bohr Hamiltonian.
- The numerical calculations for the excited energy and transition rates were calculated.
- The phase transition from spherical to axially deformed nuclei were applied for Ru-100, Pd-114, and Xe-124 nuclei.
- The phase transition from prolate to oblate shapes were applied for Os-180, Dy-162, Gd-160 nuclei.

ABSTRACT

In the present work, the eigenvalue and eigenvector has been obtained by the Bohr Hamiltonian for even-even nuclei. The competition between γ-stable and γ-rigid collective motions has been created in the presence of the rigidity parameter. The β-part of the collective potential has been chosen to be equal to the generalized Hulthen potential, while the γ-angular part of the problem is associated with Ring-shaped potential around the $\gamma = \pi/6$ and the Harmonic oscillation around the $\gamma = 0$. In both cases, the effect of rigidity and free parameters on energy spectrum of Os-180, Dy-162, Gd-160, Ru-100, Pd-114, and Xe-124 nuclei have been investigated. Also, the rates of $B(E2)$ transition have been calculated and compared with experimental data. This model has an appropriate description of energy spectra for the mentioned nuclei.

KEYWORDS

Bohr Hamiltonian
Generalized Hulthen potential
Transition rates
Ring-shaped potential
Harmonic oscillation

HISTORY

Received: 19 May 2019
Revised: 7 January 2020
Accepted: 28 January 2020
Published: October 2020

1 Introduction

In collective models of even-even nuclei, the Bohr Hamiltonian provides an appropriate tool for the description of collective quadrupole properties (Budaca and Budaca, 2015b), such as energy spectra and transition rates. These solutions can be interesting by imposing γ-rigidity parameter. The Bohr Hamiltonian has been investigated near the critical point symmetries in the nuclear structure with various potentials that are expressed in β and γ variables. The phase transition is corresponding to the breaking of the dynamical symmetries (Bonatsos et al., 2007a; Iachello, 2000, 2001a). In this discussion, the $Z(5)$ critical point symmetry is about the transition from prolate to oblate shapes. Other symmetries are $E(5)$ and $X(5)$. The $E(5)$ model specifies the second order phase transition between $U(5)$ (spherical) and $O(6)$ (γ-unstable) nuclei. The $X(5)$ model characterizes first order phase transition between $U(5)$ (spherical) and $SU(3)$ (axially deformed nuclei). Excellent discussions can be found in Refs. (Budaca and Budaca, 2015b; Bonatsos et al., 2007a; Iachello, 2000, 2001a; Chabab et al., 2015b, 2016, 2015a; Budaca and Budaca, 2015a, 2016; Hassanabadi and Alimohammadi, 2018; Bonatsos et al., 2006; Alimohammadi and Hassanabadi, 2017). The $X(5)$ model is founded on the square well potential for β-part and a harmonic oscillator potential that centered around $\gamma = 0$ in γ-part. The X(5)-β^2 model and the $Es-X(5)$ model are other attached models of $X(5)$. The γ-rigid version of $X(5)$ model (by five collective coordinates), called $X(3)$ model (by three collective coordinates) (Bonatsos et al., 2006). Two out of three collective coordinates are Euler angles and the third one is β, because there is a γ-rigid condition ($\gamma = 0$).

For example, M. Chabab et al. have studied Bohr Hamiltonian with Hulthen potential in β-part and new

*Corresponding author: Meshghi@ihu.ac.ir

generalized potential derived from a Ring-shaped in γ-part for triaxial nuclei (Chabab et al., 2015a). On the other hand, R. Budaca et al. have proposed an infinite square well potential in β-part and a harmonic oscillator form for the γ-part of potential to investigate the competition between the γ-rigid and γ-stable collective motions in the phase transition (Budaca and Budaca, 2015b).

Bohr model has been evaluated in dierent approaches such as the interplay of various shape phase conditions. In this research, we have investigated Bohr Hamiltonian with Hulthen potential for β-part in the interplay of γ-stable and γ-rigid collective motions with both the Harmonic oscillation and the Ring-shaped potentials for the γ-part. We have added two free parameters, V_0 and q, to Hulthen potential to control the depth of potential and shaped deformation. In the first part, the Harmonic oscillation around $\gamma = 0$ for the γ-part and Hulthen potential for the β-part have an interplay between γ-rigid and γ-stable collective motion in the critical point of the phase transition from spherical to axially deformed nuclei $(X(3) \cup X(5) - H)$. In the second part, the Ring-shaped potential around $\gamma = \pi/6$ for the γ-part and Hulthen potential for the β-part have an interplay between γ-rigid and γ-stable collective motion in the critical point of the phase transition from prolate to oblate nuclei $(Z(3) \cup Z(5) - H)$. We have evaluated the Bohr Hamiltonian equation with the extra term to study the competition situations by the free parameter to administer the mode of the shape variable.

Furthermore, numerical calculations for the excited energies for Os-180, Dy-162, Gd-160, Ru-100, Pd-114, and Xe-124 nuclei and $B(E2)$ transition rates of proposed models have been calculated and compared with the experimental data. This model by the rigidity parameter χ enables a better description of energy spectra for both models.

2 Theory of interplay between γ-stable and γ-rigid collective condition

2.1 Bohr Hamiltonian

The interplay between γ-stable and γ-rigid collective motions attains by (Budaca and Budaca, 2015b; Bonatsos et al., 2006; Budaca, 2014b,a):

$$H = \chi T_1 + (1-\chi)T_2 + V(\beta.\gamma) \tag{1}$$

where T_1 is the kinetic energy operator for prolate γ-rigid and T_2 is the same operator corresponding to the five-dimensional Bohr Hamiltonian. Also, $V(\beta.\gamma)$ is the potential energy operator. The rigidity degree of the systems is measured by χ parameter which is limited in $0 \leq \chi < 1$ which $\chi = 1$ associated with the prolate γ-rigid limit.

As pointed out, T_1 and T_2 operators are:

$$T_1 = -\frac{\hbar^2}{2B}\Big[\frac{1}{\beta^2}\frac{\partial}{\partial\beta}\beta^2\frac{\partial}{\partial\beta} - \frac{Q^2}{3\beta^2}\Big] \tag{2}$$

and

$$T_2 = -\frac{\hbar^2}{2B}\Big[\frac{1}{\beta^4}\frac{\partial}{\partial\beta}\beta^4\frac{\partial}{\partial\beta} + \frac{1}{\beta^2\sin(3\gamma)}\frac{\partial}{\partial\gamma}\sin(3\gamma)\frac{\partial}{\partial\gamma} - \frac{1}{4\beta^2}\sum_{k=1}^{3}\frac{Q_k^2}{\sin^2(\gamma - \frac{2}{3}\pi k)}\Big] \tag{3}$$

where B introduces the mass parameter, and Q states the angular momentum operator of the intrinsic frame with the corresponding components $Q_k (k = 1, 2, 3)$. The adapted potential for the present problem is:

$$v(\beta.\gamma) = \frac{2B}{\hbar^2}V(\beta.\gamma) = u(\beta) + (1-\chi)\frac{u(\gamma)}{\beta^2} \tag{4}$$

According to Eqs. (1) and (4), the Schrdinger equation, $H\psi(\beta,\gamma,\Omega) = E\psi(\beta,\gamma,\Omega)$, is separated into two parts as follows:

$$\Big[(1-\chi)\big[-\frac{1}{\sin(3\gamma)}\frac{\partial}{\partial\gamma}\sin(3\gamma)\frac{\partial}{\partial\gamma} + \frac{1}{4}\sum_{k=1}^{3}\frac{Q_k^2}{\sin^2(\gamma - \frac{2}{3}\pi k)}\big] + (1-\chi)u(\gamma) + \chi\frac{Q^2}{3}\Big]\varphi(\gamma,\Omega) = W\varphi(\gamma,\Omega) \tag{5}$$

and

$$\Big[-\frac{\partial^2}{\partial\beta^2} + \frac{(2\chi-4)}{\beta}\frac{\partial}{\partial\beta} + \frac{1}{\beta^2}W + u(\beta)\Big]\xi(\beta) = \varepsilon\xi(\beta) \tag{6}$$

where, the energy introduces as $\varepsilon = \frac{2B}{\hbar^2}E$, and W and ε are the eigenvalues of equations. Likewise, the total wave function is introduced by $\psi(\beta,\gamma,\Omega) = \xi(\beta)\varphi(\gamma,\Omega)$.

Now, we use the generalized Hulthen potential for the β part of total potential, Eq. (4), as follows:

$$u(\beta) = -\frac{V_0 e^{-\delta\beta}}{1 - q e^{-\delta\beta}} \tag{7}$$

where V_0 is the potential depth, q is the shaped deformation parameter, and $\delta = \frac{1}{a}$ is the screening parameter and a defines the range of the potential (Chabab et al., 2015a; Hulthén, 1942a,b).

Insertion the function of $\xi(\beta)$ as $\xi(\beta) = \beta^{x-2}f(\beta)$ in the radial equation, Eq. (6), results in:

$$\Big[\frac{\partial^2}{\partial\beta^2} - \big(\frac{A}{\beta^2} + u(\beta) - \varepsilon\big)\Big]f(\beta) = 0 \tag{8}$$

where:

$$A = W + (\chi^2 - 3\chi + 2) \tag{9}$$

By using the following expression (Chabab et al., 2015a):

$$\frac{1}{\beta^2} \approx \delta^2\frac{e^{-\delta\beta}}{(1 - q e^{-\delta\beta})^2} \tag{10}$$

and applying the new variable , also inserting Eqs. (7) and (10) into Eq. (8), we have:

$$\frac{d^2f}{dy^2} + \frac{(1-y)}{y(1-y)}\frac{df}{dy} + \Big[\frac{-A y\delta^2 + V_0 y(1-y) + q\varepsilon(1-y)^2}{q\delta^2 y^2(1-y)^2}\Big]f = 0 \tag{11}$$

To find the energy eigenvalues of Eq. (11), we use the parametric generalization of the Nikiforov-Uvarov (NU) method (Chabab et al., 2017; Nikiforov and Uvarov, 1988; Eshghi and Hamzavi, 2012; Soheibi et al., 2017; Ikhdair, 2009) as:

$$\varepsilon = -\Bigg(\frac{q\delta^2\big(n+\frac{1}{2}+\sqrt{\frac{W+(\chi^2-3\chi+2)}{q}+\frac{1}{4}}\big)^2 - V_0}{2q\delta\big(n+\frac{1}{2}+\sqrt{\frac{W+(\chi^2-3\chi+2)}{q}+\frac{1}{4}}\big)}\Bigg)^2 \tag{12}$$

where n is the principal quantum number. Equation (12) is in accordance with the energy spectrum of Ref. (Chabab et al., 2015a) for $\chi = 0$ and $q, V_0 \to 0$ values. According to NU method, the wave function is given by:

$$\begin{aligned} f(y) =& N y^{\sqrt{\frac{-\varepsilon}{\delta^2}}}(1-y)^{\frac{1}{2}+\sqrt{\frac{A}{4}+\frac{1}{4}}} \\ &\times P_n^{(2\sqrt{\frac{-\varepsilon}{\delta^2}}, 2\sqrt{\frac{A}{4}+\frac{1}{4}})}(1-2y) \end{aligned} \tag{13}$$

The normalization constant of β part can be calculated from the normalization condition as follow:

$$\int_0^\infty \xi^2(\beta)\beta^{4-2\chi}\mathrm{d}\beta = 1 \tag{14}$$

In this section, we calculate energy eigenvalues and wave functions in the principal quantum number (n), systems rigidity parameter (χ), and the separation constant (W). It is known that n can be changed by change of bands, and $n\chi$ is limited in $0 \le \chi < 1$. But for calculation of W in the angular part of the Hamiltonian (Eq. (5)), we select two following potentials for the deformed shape nuclei to achieve the final energy spectrum in two approaches.

2.2 *The Harmonic oscillator potential around* $\gamma = 0$

To solve Eq. (5), the rotational term of this equation has been approximated in the prolate axial nuclei as (Budaca and Budaca, 2015b; Iachello, 2001b):

$$\sum_{k=1}^{3}\frac{Q_k^2}{\sin^2(\gamma-\frac{2}{3}\pi k)} \approx \frac{4}{3}Q^2 + Q_3^2\big(\frac{1}{\sin^2(\gamma)}-\frac{4}{3}\big) \tag{15}$$

In this case, we can separate the γ and angular variables by $\varphi(\gamma,\Omega) = \eta(\gamma)\mathcal{D}^L_{MK}(\Omega)$, where $\mathcal{D}^L_{MK}(\Omega)$ is the Wigner function, and L, M and K represent the total angular momentum, its projections on the body-fixed and laboratory-fixed z-axis, respectively. The following equation is derived for the γ shape variable:

$$\big[-\frac{1}{\sin(3\gamma)}\frac{\partial}{\partial\gamma}\sin(3\gamma)\frac{\partial}{\partial\gamma}+\frac{K^2}{4\sin^2(\gamma)}+u(\gamma)\big]\eta(\gamma) = \varepsilon_\gamma\eta(\gamma) \tag{16}$$

with:

$$\varepsilon_\gamma = \frac{1}{(1-\chi)}\big[W - \frac{L(L+1)-(1-\chi)K^2}{3}\big] \tag{17}$$

By considering $u(\gamma)$ as:

$$u(\gamma) = (3c)^2\frac{\gamma^2}{2} \tag{18}$$

we get a hypothesis of small oscillations around $\gamma = 0$ that pause at $\chi = 1$. The parameter of c is defined the string constant of the oscillator that demonstrates the stiffness of the γ vibrations. By applying a harmonic approximation for the trigonometric functions around $\gamma = 0$, we have:

$$\big[-\frac{1}{\gamma}\frac{\partial}{\partial\gamma}\gamma\frac{\partial}{\partial\gamma}+\frac{K^2}{4\gamma^2}+u(\gamma)\big]\eta(\gamma) = \varepsilon_\gamma\eta(\gamma) \tag{19}$$

The solutions are readily obtained in terms of the Laguerre polynomials (Budaca and Budaca, 2015b; Chabab et al., 2016):

$$n_{n_\gamma,|K|}(\gamma) = N_{\tilde{n}_\gamma,|K|}\gamma^{|K/2|}\exp(-3c\frac{\gamma^2}{2})L^{|K/2|}_{\tilde{n}_\gamma}(3c\gamma^2) \tag{20}$$

where $\tilde{n}_\gamma = (n_\gamma, |K/2|)/2$, $L^{|K/2|}_{\tilde{n}_\gamma}$ represents the Laguerre polynomial, and $N_{n_\gamma,|K|}(\gamma)$ is a normalization constant that is specified from the normalization condition as:

$$\int_0^{\pi/3}\eta^2_{n_\gamma,|K|}(\gamma)|\sin(3\gamma)|\mathrm{d}\gamma = 1 \tag{21}$$

In Eq. (19), we used $|\sin(3\gamma)| = |3\gamma|$ in the small γ vibration, so the integral can be solvable (Chabab et al., 2016, 2017):

$$N_{\tilde{n}_\gamma,|K|} = \big[\frac{2}{3}(3c)^{1+|K/2|}\frac{\tilde{n}_\gamma!}{\Gamma(\tilde{n}_\gamma+1+|K/2|)}\big]^{\frac{1}{2}} \tag{22}$$

where n_γ is the quantum number related to γ-excitation. For states of $(n_\gamma, K) = (0,0)$ and $(n_\gamma, K) = (1,2)$, the normalization constants are calculated as:

$$N^2_{0,0} = 2c \quad \text{and} \quad N^2_{1,2} = 6c^2 \tag{23}$$

where $\dfrac{N^2_{0,0}}{N^2_{1,2}} = \dfrac{1}{3c}$.

Therefore, the corresponding eigenvalues are:

$$\varepsilon_\gamma = 3c(n_\gamma+1), \quad n_\gamma = 0,1,2,... \tag{24}$$

with:

$$K = \begin{cases} 0, \pm 2n_\gamma & \text{for even } n_\gamma \\ \pm n_\gamma & \text{for odd } n_\gamma \end{cases} \tag{25}$$

We obtain W by a combination of Eqs. (17) and (24):

$$W = (1-\chi)3c(n_\gamma+1) + \frac{L(L+1)-(1-\chi)K^2}{3} \tag{26}$$

Therefore, in our calculations, the total wave function is obtained as follows:

$$\begin{aligned} &\psi_{LMknn_\gamma}(\beta,\gamma,\Omega) = \varepsilon_{LKnn_\gamma}(\beta)\eta_{n_\gamma,|K|}(\gamma) \\ &\times\sqrt{\frac{2L+1}{16\pi^2(1+\delta_{k,0})}}[\mathcal{D}^L_{MK}(\Omega)+(-1)^L\mathcal{D}^L_{M-K}(\Omega)] \end{aligned} \tag{27}$$

In the general case, the quadrupole operator is defined as:

$$\begin{aligned} T^{(E2)}_M = t\beta\big[&\mathcal{D}^2_{M,0}(\Omega)\cos(\gamma)+ \\ &\frac{1}{\sqrt{2}}\big(\mathcal{D}^2_{M,2}(\Omega)+\mathcal{D}^{-2}_{M,0}(\Omega)\big)\cos(\gamma)\big] \end{aligned} \tag{28}$$

where t is a scale factor. By means of the above functions, we can compute the $B(E2)$ transition rates.

The $B(E2)$ transition rates from an initial to a final state are given by (Budaca and Budaca, 2015b; Chabab et al., 2016; Bijker et al., 2003; Bonatsos et al., 2007b):

$$B(E2; L_i\ K_i\ n_i\ n_{\gamma i} \to L_f\ K_f\ n_f\ n_{\gamma f}) = \frac{5t^2}{16\pi}\langle L_i, k_i; 2, k_i - k_f | L_f, k_f\rangle^2 I^2_{n_i L_i, n_f L_f} C^2_{n_{\gamma i} K_i, n_{\gamma f} K_f} \tag{29}$$

where, the first term is the Clebsch-Gordan coefficient and dictating the angular momentum selection rules. I is the integral over β variable:

$$I_{n_i L_i, n_f L_f} = \int_0^\infty \beta \xi_{L_i K_i n_i n_{\gamma i}} \xi_{L_f K_f n_f n_{\gamma f}} \beta^{4-2\chi} \mathrm{d}\beta \tag{30}$$

and also, $C_{n_{\gamma i} K_i, n_{\gamma f} K_f}$ is the integral over γ variable and has the form (Chabab et al., 2016):

$$C_{n_{\gamma i} K_i, n_{\gamma f} K_f} = \int_0^{\pi/2} \sin(\gamma) \eta_{n_{\gamma i}, |K|_i} \eta_{n_{\gamma f}, |K|_f} |\sin(3\gamma)| \mathrm{d}\gamma \tag{31}$$

For the transitions ($g \to g, \beta \to \beta, \gamma \to \gamma$, and $\beta \to g$) with $\Delta k = 0$, the γ-integral part is reduced to the orthonormality condition of the γ-wave functions $C_{n_{\gamma i} K_i, n_{\gamma f} K_f} = \delta_{n_{\gamma i}, n_{\gamma f} K_f} \delta_{K_i, K_f}$.

Also, for the transitions ($\gamma \to g, \gamma \to \beta$) with $\Delta k = 2$, and by using the approximation $|\sin(3\gamma)| = 3|\gamma|$, Eq. (31) recasts to:

$$C_{n_{\gamma i} K_i, n_{\gamma f} K_f} = \frac{2(3c)^{1+\frac{|k_i|}{4}+\frac{|k_f|}{4}}}{(\Gamma(1+\frac{|k_i|}{4})\Gamma(1+\frac{|k_f|}{4}))^{\frac{1}{2}}} \times \int_0^{\pi/3} \gamma^{2+\frac{|k_i|}{2}+\frac{|k_f|}{2}} \mathrm{e}^{-3c\gamma^2} \mathrm{d}\gamma \tag{32}$$

where the Laguerre polynomials are unity since $\tilde{n}_\gamma = 0$. For $(n_\gamma, k) = (1, 2) \to (0, 0)$ transition, Eq. (32) results in:

$$C_{0,0;1,2} = \frac{1}{\sqrt{3c}}. \tag{33}$$

2.3 The Ring-shaped potential around $\gamma = \frac{\pi}{6}$

According to Ref. (Chabab et al., 2015a), we propose Ring-shaped potential for the γ variable part of Hamiltonian with a minimum at $\gamma = \frac{\pi}{6}$ as:

$$u(\gamma) = \frac{c + s\cos^2(3\gamma)}{\sin^2(3\gamma)} \tag{34}$$

By means of its expansion around $\gamma = \frac{\pi}{6}$ and for a small value of the parameter s in comparison with the parameter c, $\frac{s}{c} \ll 1$. We recover the Harmonic oscillator with an additive constant which is also widely used in this case:

$$u(\gamma) \approx \frac{1}{2}(\frac{9}{2}c)\big(\gamma - \frac{\pi}{6}\big)^2 + \tilde{c} \tag{35}$$

where $\tilde{c}$ is the additive constant. Inserting Eq. (34) in Eq. (5), one gets:

$$\begin{aligned}(1-\chi)\Big[&-\frac{1}{\sin(3\gamma)}\frac{\partial}{\partial\gamma}\sin(3\gamma)\frac{\partial}{\partial\gamma} + \frac{1}{4}\sum_{k=1}^{3}\frac{Q_k^2}{\sin^2(\gamma - \frac{2}{3}\pi k)} \\ &+ \frac{c + s\cos^2(3\gamma)}{\sin^2(3\gamma)}\Big]\varphi(\gamma,\Omega) + \chi\frac{Q^2}{3}\varphi(\gamma,\Omega) \\ &= W\varphi(\gamma,\Omega)\end{aligned} \tag{36}$$

Now, we again separate the and angular variables by $\varphi(\gamma, \Omega) = \eta(\gamma)\mathcal{D}^L_{M\alpha}(\Omega)$, where L, M, and α are total angular momentum quantum number, quantum number of the projections of angular momentum on the laboratory fixed z-axis, and the body-fixed x'-axis, respectively. Also, there is a wobbling quantum number n_w that depends on α by $n_w = L - \alpha$. In the triaxial nuclei, the rotational term of Eq. (36) is (Chabab et al., 2015a; Fortunato, 2004; Bonatsos et al., 2004a):

$$\frac{1}{4}\sum_{k=1}^{3}\frac{Q_k^2}{\sin^2(\gamma - \frac{2}{3}\pi k)} \approx Q^2 - \frac{3}{4}Q_1^2 \tag{37}$$

The last approximation leads to:

$$(Q^2 - \frac{3}{4}Q_1^2)\mathcal{D}^L_{M\alpha}(\Omega) = \Lambda_1 \mathcal{D}^L_{M\alpha}(\Omega) \tag{38}$$

where $\Lambda_1 = L(L+1) - \frac{3}{4}\alpha^2$ (Chabab et al., 2016), so remaining terms of Eq. (36) lead to:

$$\Big[-\frac{1}{\sin(3\gamma)}\frac{\partial}{\partial\gamma}\sin(3\gamma)\frac{\partial}{\partial\gamma} + \frac{c + s\cos^2(3\gamma)}{\sin^2(3\gamma)}\Big]\eta(\gamma) = \Lambda_2\eta(\gamma) \tag{39}$$

As pointed out in Ref. (Chabab et al., 2015a), eigenvalues of the last equation is $\Lambda_2 = 9n_\gamma(n_\gamma + 1) + 3\sqrt{c+s}(2n_\gamma + 1) + c)$. Finally, eigenvalue of Eq. (5) will be obtained by:

$$\begin{aligned}W =&(1-\chi)[\Lambda_1 + \Lambda_2] + \chi\frac{L(L+1)}{3} \\ =&(1-\chi)\Big[9n_\gamma(n_\gamma+1) + 3\sqrt{c+s}(2n_\gamma+1) + c \\ &+ \frac{L(L+4) + 3n_w(2L - n_w)}{4}\Big] + \chi\frac{L(L+1)}{3}\end{aligned} \tag{40}$$

Eigenfunctions of γ variable are given in terms of Legendre polynomials:

$$\eta(\gamma) = N_{n_\gamma} P^{\frac{1}{6}\sqrt{c+s}}_{n_\gamma + \frac{1}{6}\sqrt{c+s}}(z) \tag{41}$$

where $z = \cos(3\gamma)$ and, N_{n_γ} is obtained by:

$$\int_0^{\pi/3} \eta^2_{n_\gamma, |K|}(\gamma)|\sin(3\gamma)|\ \mathrm{d}\gamma = 1 \tag{42}$$

In this case, we get the normalization condition as:

$$N_{n_\gamma} = \sqrt{\frac{3}{2}\frac{(2\big(n_\gamma + \frac{1}{6}\sqrt{c+s}\big) + 1)(n_\gamma!)}{(\frac{1}{6}\sqrt{c+s} + n_\gamma)!}} \tag{43}$$

Finally, the total wave function is given by:

$$\psi_{LM\alpha nn_\gamma}(\beta,\gamma,\Omega)=\xi_{LM\alpha nn_\gamma}(\beta)\eta_{n_\gamma}(\gamma)\times \sqrt{\frac{2L+1}{16\pi^2(1+\delta_{\alpha,0})}}[\mathcal{D}^L_{M\alpha}(\Omega)+(-1)^L\mathcal{D}^L_{M-\alpha}(\Omega)] \quad (44)$$

Both sections in energy eigenvalues and wave functions have the same β part, according to Eqs. (12) and (13), but are different in separation constant of and part wave functions. We also can easily calculate the $B(E2)$ transition rates with the above equations. The quadrupole operator is determined by (Chabab et al., 2015a; Edmonds, 1996):

$$T^{(E2)}_M = t\beta\big[\mathcal{D}^2_{M.0}(\Omega)\cos(\gamma-\frac{2\pi}{3})+ \frac{1}{\sqrt{2}}\big(\mathcal{D}^2_{M.2}(\Omega)+\mathcal{D}^{-2}_{M.-2}(\Omega)\big)\sin(\gamma-\frac{2\pi}{3})\big] \quad (45)$$

where t denotes the scale factor. The quadrupole operator changes to the following equation for triaxial nuclei around $\gamma=\frac{\pi}{6}$:

$$T^{(E2)}_M = t\beta\frac{1}{\sqrt{2}}\big(\mathcal{D}^{(2)}_{M.2}(\Omega)+\mathcal{D}^{(-2)}_{M.-2}(\Omega)\big) \quad (46)$$

Now, by means of the wave function, we can calculate $B(E2;L_i\alpha_i\to L_f\alpha_f)$ transition rates from an initial to a final state:

$$B(E2;L_i\alpha_i\to L_f\alpha_f)=\frac{5}{16\pi}\frac{|\langle L_f\alpha_f||T^{(E2)}||L_i\alpha_i\rangle|^2}{(2L_i+1)} \quad (47)$$

The Wigner-Eckart theorem cause to reduced matrix element as:

$$\langle L_fM_f\alpha_f||T^{(E2)}||L_iM_i\alpha_i\rangle = \frac{(L_i2L_f|M_iMM_f)}{\sqrt{2L_f+1}}\langle L_f\alpha_f||T^{(E2)}||L_i\alpha_i\rangle \quad (48)$$

The $B(E_2)$ transition rates turn into the following general expression:

$$\begin{aligned}B(E2;L_i\alpha_i\to L_f\alpha_f) = \frac{5}{16\pi}\frac{t^2}{2}&\frac{1}{(1+\delta_{\alpha_i,0})(1+\delta_{\alpha_f,0})}\\ &\times[(L_i2L_f|\alpha_i2\alpha_f)+(L_i2L_f|\alpha_i-2\alpha_f)\\ &+(-1)^L(L_i2L_f|\alpha_i-2-\alpha_f)]^2\\ &\times[I_\beta(n_i,L_i,\alpha_i;n_f,L_f,\alpha_f)]^2\end{aligned} \quad (49)$$

In the above equation, integral over β is given by:

$$I_\beta(n_i,L_i,\alpha_i;n_f,L_f,\alpha_f)= \int_0^\infty \beta\xi_{n_i,L_i,\alpha_i}(\beta)\xi_{n_f,L_f,\alpha_f}(\beta)\beta^{4-2\chi}\mathrm{d}\beta \quad (50)$$

It was confronted by three Clebsch-Gordan coefficients that lead to $\Delta\alpha=\pm2$ transition rule. The three coefficients involve $\alpha_i+2=\alpha_f$, $\alpha_i-2=\alpha_f$ and $\alpha_i+\alpha_f=2$, respectively. The ground-state band (gsb) is specified by $n=0$, $n_\gamma=0$, and $n_w=0$ so $\alpha_i=L_i$ and $\alpha_f=L_f$. Detailed discussions on the $B(E2)$ rates have been presented in Ref. (Bonatsos et al., 2004b).

3 Numerical results and discussions

Having the continual deformed shape and collective properties, Os-180, Dy-162, Gd-160, Ru-100, Pd-114, and Xe-124 nuclei have been studied so far. For example, see the evaluations of Refs. (Budaca and Budaca, 2015b; Hassanabadi and Alimohammadi, 2018; Alimohammadi and Hassanabadi, 2017). In the above sections, we have calculated equations of the energy spectra and $B(E2)$ transition rates by means of the generalized Hulthen potential for the β part. However, in the angular part of the Hamiltonian, we have selected two ways for deformed shape nuclei to achieve the final energy spectrum.

The mentioned nuclei have been evaluated by tting their experimental energy spectrum for ground, β, and bands with the calculated formula and normalized to the corresponding energy of the rst excited state. Therefore, the nuclei have been discovered to have the smallest deviations from the experimental data by the root mean square (rms) deviation formula:

$$\sigma=\sqrt{\frac{\sum_{i=1}^m(E_{i(exp)}-E_{i(th)})^2}{(m-1)E(2_1^+)^2}} \quad (51)$$

The experimental and obtained energies of the i^{th} level are specifying by $E_{i(exp)}$ and $E_{i(th)}$, respectively, where $E(2_1^+)$ is the energy of the initial excited level of the ground-state band and m shows the number of states involved in the fitting. The results corresponding to the fit are presented in Tables 1 and 2.

3.1 *Results for the Harmonic oscillator potential around* $\gamma=0$

The Harmonic oscillator potential is applied for Ru-100, Pd-114, and Xe-124 nuclei in Sec. (2.2). In Eq. (27), all ground states, β and γ bands are labeled by the set of quantum numbers, K, n, n_γ, L and uniquely identify this model. The lowest bands are (Budaca and Budaca, 2015b; Bijker et al., 2003):

1. The ground-state band is determined by $K=0,n=0,n_\gamma=0$.
2. The band is distinguished by $K=0,n=1,n_\gamma=0$.
3. The band is specified by $K=2,n=0,n_\gamma=1$.

According to Table 1, σ values (rms) of Dy-162 and Gd-160 nuclei are small against those reported the Ref. (Budaca and Budaca, 2015b). Therefore, there is an acceptable agreement between the calculated values and experimental data. This agreement is due to a number of free parameters of the potentials for β part and angular part of the Hamiltonian against the Ref. (Budaca and Budaca, 2015b) with only two free parameters. It is the advantage of our calculations compared with other works.

We have also computed the transition rates for the nuclei in Table 3 by means of Eq. (29). There is an agreement between some theoretical and experimental values.

Table 1: Comparison of theoretical predictions and experimental data for the ground state, β, and γ bands normalized to the $E(2_g^+)$ state for Os-180, Dy-162, and Gd-160 nuclei.

	Gd-160		Dy-162		Os-180	
	Our work	Exp.	Our work	Exp.	Our work	Exp.
$R_{\frac{4_g^+}{2_g^+}}$	3.31	3.301	3.30	3.29	3.310	3.09
$R_{\frac{6_g^+}{2_g^+}}$	6.88	6.84	6.84	6.80	6.87	6.802
$R_{\frac{8_g^+}{2_g^+}}$	11.65	11.53	11.56	11.42	11.65	9.52
$R_{\frac{10_g^+}{2_g^+}}$	17.60	17.28	17.41	17.05	17.64	13.38
$R_{\frac{12_g^+}{2_g^+}}$	24.68	24.00	24.36	24.57	24.81	17.48
$R_{\frac{14_g^+}{2_g^+}}$	32.87	31.59	32.39	30.89	33.17	21.76
$R_{\frac{0_\beta^+}{2_g^+}}$	18.03	18.33	19.77	20.66	4.19	5.57
$R_{\frac{2_\beta^+}{2_g^+}}$	19.44	19.08	21.25	21.43	5.44	6.29
$R_{\frac{4_\beta^+}{2_g^+}}$	22.67	-	24.61	23.39	8.26	7.97
$R_{\frac{2_\gamma^+}{2_g^+}}$	12.82	13.13	10.52	11.07	6.60	6.59
$R_{\frac{3_\gamma^+}{2_g^+}}$	13.76	14.05	11.46	11.49	7.57	7.74
$R_{\frac{4_\gamma^+}{2_g^+}}$	15.01	15.25	12.70	13.15	8.85	9.06
$R_{\frac{5_\gamma^+}{2_g^+}}$	16.57	16.76	14.25	14.66	10.44	10.64
$R_{\frac{6_\gamma^+}{2_g^+}}$	18.43	18.51	16.09	16.43	12.34	12.32
$R_{\frac{7_\gamma^+}{2_g^+}}$	20.59	20.58	18.23	18.48	14.55	14.24
$R_{\frac{8_\gamma^+}{2_g^+}}$	23.05	22.81	20.65	20.71	17.07	-
$R_{\frac{9_\gamma^+}{2_g^+}}$	25.80	-	23.36	23.28	19.89	18.25
$R_{\frac{10_\gamma^+}{2_g^+}}$	28.84	28.14	26.35	25.88	23.01	-
$R_{\frac{11_\gamma^+}{2_g^+}}$	32.17	-	29.62	28.98	26.43	-
$R_{\frac{12_\gamma^+}{2_g^+}}$	35.79	34.31	33.17	32.52	30.14	-
χ	0.55	-	0.29	-	0.74	-
c	18.44	-	9.69	-	15.32	-
δ	3.91	-	1.22	-	9.72	-
q	7.94	-	10.21	-	1.10	-
V_0	5.20	-	0.25	-	32.10	-
σ	0.34	-	0.63	-	1.60	-

3.2 Results for the Harmonic oscillator potential around $\gamma = \frac{\pi}{6}$

The Ring-shaped potential is used for Os-180, Dy-162, and Gd-160 nuclei in Sec. (2.3). In Eq. (44), all ground states, β, and γ bands are labeled by the set of quantum numbers, n, n_γ, n_w, L, and the lowest bands are (Chabab et al., 2015a; Greiner and Maruhn, 1996):

1. The ground-state band is composed by $n = 0, n_\gamma = 0, n_w = 0$.
2. The band is distinguished by $n = 1, n_\gamma = 0, n_w = 0$.
3. The band is characterized by $n = 0, n_\gamma = 0$ but $n_w = 2$ for even L levels and $n_w = 1$. for odd L levels.

In Table 2, σ values (rms) of Ru-100, Pd-114 and Xe-124 nuclei are small in comparison with those reported in Ref. (Alimohammadi and Hassanabadi, 2017). Therefore, there is good agreement between the calculated values and experimental data. In addition, this good agreement is a results of the quantum numbers. For example, in Ref. (Alimohammadi and Hassanabadi, 2017), quantum numbers are s, τ and ?, so the energy of different quantum numbers of the levels is the same. However, in the present work, the Ring-shaped potential for γ part enables us to separate energy for every special even and odd levels.

We have also computed the transition rates for the nuclei given in Table 4 by using Eq. (49). There is an agreement between some theoretical and experimental values.

3.3 Results of other calculation

The special kind of diagram, which depends on χ, has been investigated in Ref. (Budaca and Budaca, 2015a). In their calculations, there are two free parameters besides χ, so they can compare variations of the parameter in the different diagrams. But our total energy has more than two free parameters. We have plotted this diagram for the some nuclei using their obtained parameters as shown in Tables 1 and 2.

As it is obvious, the reported calculations in the last sections have some free parameters, such as constant factor V_0, shape deformation parameter q, screening parameter δ, and the rigidity parameter χ, that are the same for both subsection. The others are stiffness of the γ oscillations in subsection 2.2, and c and s are free parameters that mentioned in subsection 2.3. The effect of the free parameters on the total energy of system has been evaluated by the mentioned equations. The dependence of the system's energy in χ that normalized to the two first ground-state bands are shown in Figs. 1 to 6 for different nuclei. According to Figs. 1 to 3 for Os-180, Gd-160, and Dy-162 nuclei, the ground states are not strongly influenced by χ. While the behavior of the β bands is fundamentally the same as in the ground band case, there is a difference between their β and γ-bands. It means that the γ-bands are more influenced than β-band by χ, and γ-bands are more variable in energy.

In Figs. 4 to 6, the behavior of all bands and dependence of the system's energy in χ are closed to each other. According to Table 2, the value of χ is around 0.5, and energy in $\chi \to 1$ for all figures and all bands vanishes. Because the Ring-shaped potential is an appropriate potential for γ-stable models, so this potential has better agreement with experimental data for $\chi < 0.5$.

Table 2: Comparison of theoretical predictions and experimental data for the ground state, β, and γ bands normalized to the $E(2_g^+)$ state for Ru-100, Pd-114, and Xe-124 nuclei.

	Pd-114		Ru-100		Xe-124	
	Our work	Exp.	Our work	Exp.	Our work	Exp.
$R_{\frac{4_g^+}{2_g^+}}$	2.65	2.56	2.53	2.27	2.64	2.48
$R_{\frac{6_g^+}{2_g^+}}$	4.61	4.51	4.20	3.85	4.60	4.37
$R_{\frac{8_g^+}{2_g^+}}$	6.58	6.66	5.78	5.67	6.64	6.58
$R_{\frac{10_g^+}{2_g^+}}$	8.40	8.60	7.14	7.85	8.56	8.96
$R_{\frac{0_\beta^+}{2_g^+}}$	2.99	2.62	2.40	2.10	3.70	3.58
$R_{\frac{2_\beta^+}{2_g^+}}$	3.78	4.18	3.16	3.46	4.46	4.60
$R_{\frac{2_\beta^+}{2_g^+}}$	5.07	-	4.33	4.36	5.70	5.69
$R_{\frac{2_\gamma^+}{2_g^+}}$	1.58	2.09	1.62	2.52	1.64	2.39
$R_{\frac{3_\gamma^+}{2_g^+}}$	2.42	3.04	2.40	3.49	2.50	3.59
$R_{\frac{4_\gamma^+}{2_g^+}}$	4.01	3.97	3.85	3.82	4.18	4.06
$R_{\frac{5_\gamma^+}{2_g^+}}$	4.54	4.90	4.25	4.78	4.66	5.19
$R_{\frac{6_\gamma^+}{2_g^+}}$	6.30	5.94	5.73	5.01	6.57	6.06
$R_{\frac{7_\gamma^+}{2_g^+}}$	6.60	6.88	5.90	6.39	6.80	7.27
$R_{\frac{8_\gamma^+}{2_g^+}}$	8.31	7.98	7.24	6.58	8.70	8.23
χ	0.47	-	0.40	-	0.40	-
c	59.29	-	29.88	-	55.00	-
s	1.73	-	20.49	-	22.77	-
δ	0.22	-	0.10	-	0.10	-
q	0.37	-	0.35	-	0.56	-
V_0	34.75	-	31.87	-	41.68	-
σ	0.35	-	0.58	-	0.48	-

Table 3: Comparison of theoretical predictions and experimental data of $B(E2)$ transition rates for Os-166, Gd-180, and Dy-162 nuclei.

$B(E2)$	Os-166		Gd-180		Dy-162	
	Our work	Exp.	Our work	Exp.	Our work	Exp.
$\frac{4_g^+ \to 2_g^+}{2_g^+ \to 0_g^+}$	1.38	1.45	1.41	-	1.42	1.42
$\frac{6_g^+ \to 4_g^+}{2_g^+ \to 0_g^+}$	1.47	1.15	1.54	-	1.53	1.48
$\frac{2_\gamma^+ \to 2_g^+}{2_\gamma^+ \to 0_g^+}$	1.42	-	1.43	1.87	1.42	1.78
$\frac{2_\gamma^+ \to 4_g^+}{2_\gamma^+ \to 0_g^+}$	0.06	-	0.06	0.189	0.07	0.137

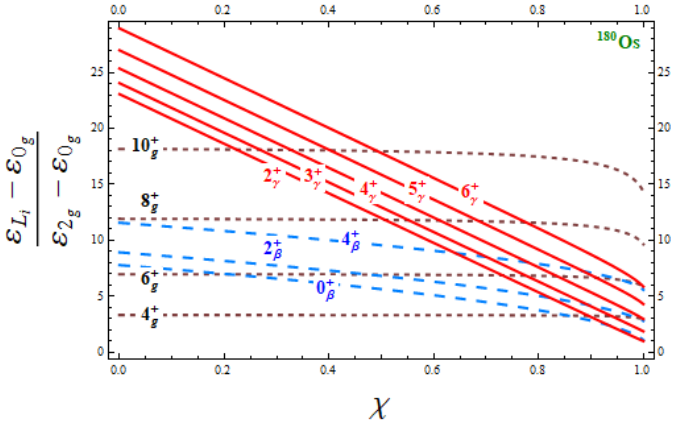

Figure 1: The low-lying energy spectrum (vertical axis) given as function of the rigidity parameter χ (horizontal axis) for Os-180. The ground band energy curves are visualized as dotted lines, the β bands are shown by dashed lines, and the solid lines are associated to the γ band states.

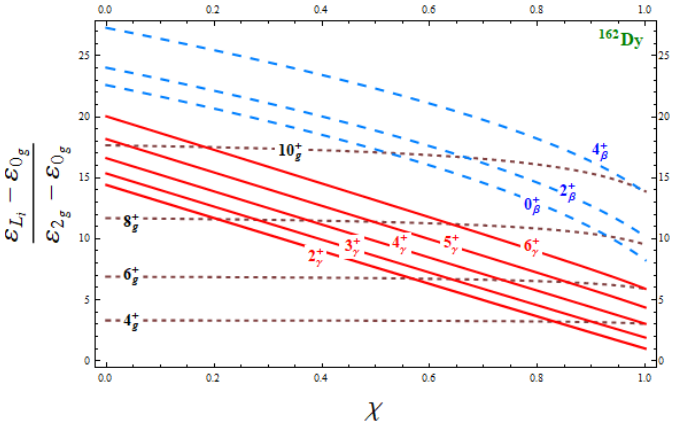

Figure 2: The low-lying energy spectrum (vertical axis) given as function of the rigidity parameter χ (horizontal axis) for Dy-162. The ground band energy curves are visualized as dotted lines, the β bands are shown by dashed lines, and the solid lines are associated to the γ band states.

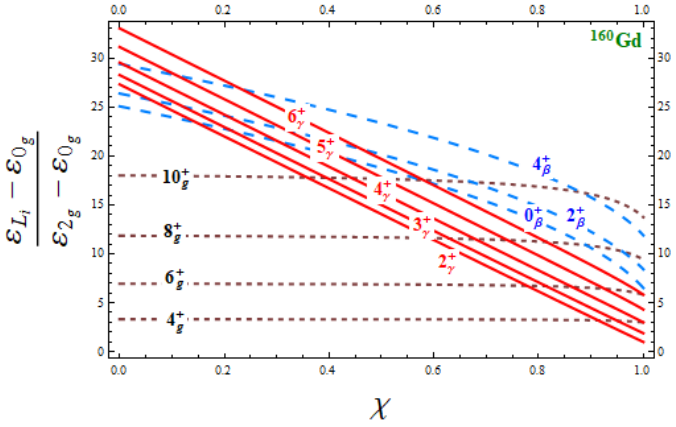

Figure 3: The low-lying energy spectrum (vertical axis) given as function of the rigidity parameter χ (horizontal axis) for Gd-160. The ground band energy curves are visualized as dotted lines, the β bands are shown by dashed lines, and the solid lines are associated to the γ band states.

Table 4: Comparison of theoretical predictions and experimental data of $B(E2)$ transition rates for Pd-114, Ru-100, and Xe-124 nuclei.

$B(E2)$	Pd-114		Ru-100		Xe-124	
	Our work	Exp.	Our work	Exp.	Our work	Exp.
$\frac{4_g^+ \to 2_g^+}{2_g^+ \to 0_g^+}$	1.30	-	1.30	1.4±0.1	1.35	1.17
$\frac{6_g^+ \to 4_g^+}{2_g^+ \to 0_g^+}$	1.49	-	1.52	<4.6±0.1	1.60	1.52±0.10
$\frac{8_g^+ \to 6_g^+}{2_g^+ \to 0_g^+}$	1.48	-	1.58	-	1.69	1.14±0.33
$\frac{10_g^+ \to 8_g^+}{2_g^+ \to 0_g^+}$	1.40	-	1.59	-	1.71	0.36±0.04
$\frac{2_\gamma^+ \to 2_g^+}{2_g^+ \to 0_g^+}$	1.42	-	1.45	0.9	1.43	0.55±0.09
$\frac{4_\gamma^+ \to 4_g^+}{2_g^+ \to 0_g^+}$	0.25	-	0.50	0.8±0.5	0.26	0.58±0.21
$\frac{4_\gamma^+ \to 2_\gamma^+}{2_g^+ \to 0_g^+}$	0.50	-	0.48	-	0.54	1.2±0.4
$\frac{3_\gamma^+ \to 2_\gamma^+}{2_g^+ \to 0_g^+}$	1.74	-	1.78	0.3±0.1	1.77	0.16±0.06

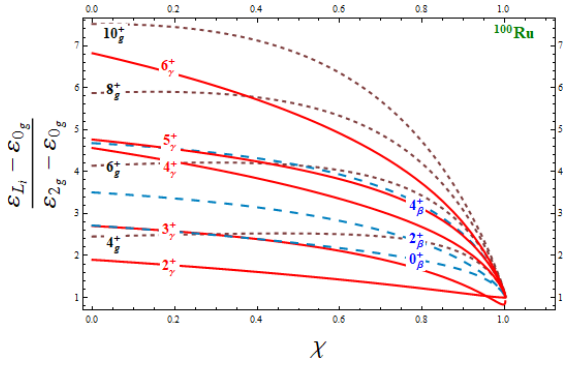

Figure 4: The low-lying energy spectrum (vertical axis) given as function of the rigidity parameter χ (horizontal axis) for Ru-100. The ground band energy curves are visualized as dotted lines, the β bands are shown by dashed lines, and the solid lines are associated to the γ band states.

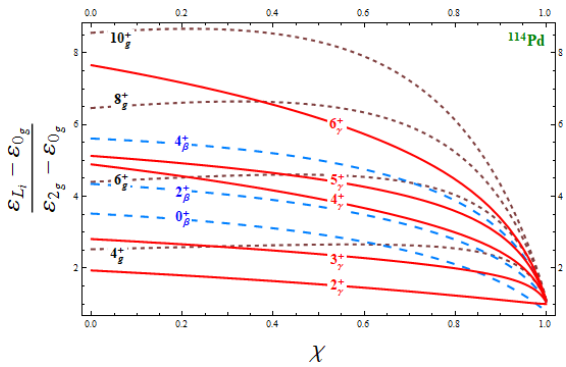

Figure 5: The low-lying energy spectrum (vertical axis) given as function of the rigidity parameter χ (horizontal axis) for Pf-114. The ground band energy curves are visualized as dotted lines, the β bands are shown by dashed lines, and the solid lines are associated to the γ band states.

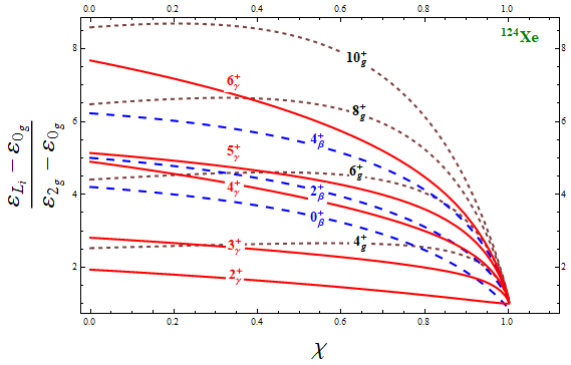

Figure 6: The low-lying energy spectrum (vertical axis) given as function of the rigidity parameter χ (horizontal axis) for Xe-124. The ground band energy curves are visualized as dotted lines, the β bands are shown by dashed lines, and the solid lines are associated to the γ band states.

On the other hand, the ratio of the excited states of a ground band that have been normalized to the energy of the rst excited state is used to dene the range of a rotational deformed and vibrational deformed which are 3.33 and 2.00, respectively. According to the results, Os-180, Gd-160, and Dy-162 nuclei follow the rotational models. Also, Pd-114, Ru-100 and Xe-124 nuclei conform vibrational models.

We have investigated another sensitive signature for triaxiality and axially symmetric structure, that is clearly the odd-even staggering of the level energies within the γ-band. It can be obtained by (Chabab et al., 2015a):

$$S(J) = \frac{E(J_\gamma^+) + E((J-2)_\gamma^+) - 2E((J-1)_\gamma^+)}{E(2_1^+)} \qquad (52)$$

Such a quantity measures the displacement of the $(J-1)_\gamma^+$ level relatively to the average of its neighbors, J_γ^+ and

$(J-2)^+_\gamma$, normalized to the energy of the first excited state of the ground band, $E(2^+_1)$. According to Ref. (Chabab et al., 2015a), it has been found that γ-soft shapes exhibit staggering whit negative $S(J)$ values at even-J and positive $S(J)$ values at odd-J spins. We plotted the function of $S(J)$ for both triaxiality and axially symmetric structure in Figs. 7 and 8. As shown in Fig. 8, there is a strong odd-even staggering of theoretical values for every three isotopes. It has been discovered that in the γ-band, this reflux of the odd states with the even states can be regarded as a strange signature of these solutions and as an examination whether these models are realistic. But this occurs for triaxial nuclei and not for axially symmetric prolate ones. Note that in the axially symmetric prolate state k is a good quantum number. This quantum number for the ground and β bands is zero and for the γ band is two, where both of them are constant. Because of constant value of k, in Fig. 7, $S(J)$ values of the even and odd state energies are not very different from each other. But for triaxial nuclei, α is a good quantum number and is not constant. For the ground and β bands $\alpha = L$ and for odd and even states of γ band are $\alpha = L-1$ and $\alpha = L-2$ respectively, then the α contributes more to the even state energies than to the odd ones and generating this reverse effect.

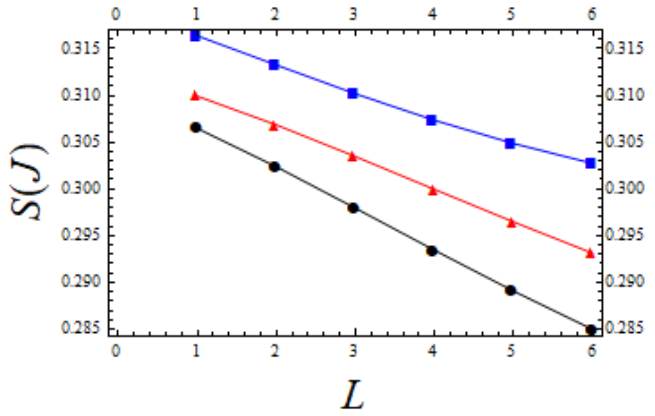

Figure 7: The theoretical values for staggering behavior of Os-180 (Blue), Gd-160 (Red), and Dy-162 (Black) nuclei.

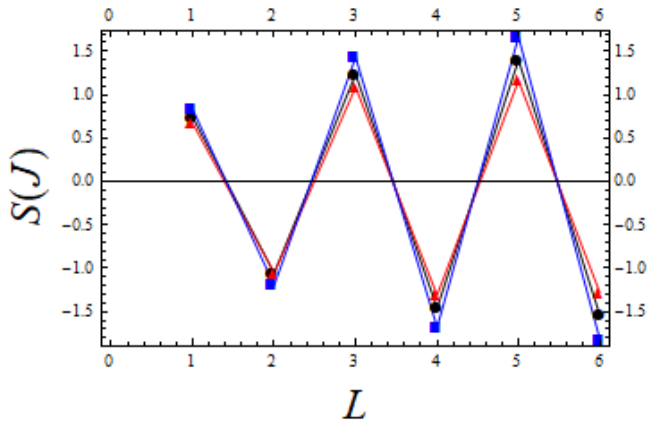

Figure 8: The theoretical values for staggering behavior of Ru-100 (Red), Pd-114 (Black), and Xe-124 (Blue) nuclei.

4 Conclusion

In this work, we solved the Bohr Hamiltonian with a generalized Hulthen potential for the β-part, in the interplay of γ-stable and γ-rigid collective motions with both the Harmonic oscillation around $\gamma = 0$ and the Ring-shaped potentials around $\gamma = \frac{\pi}{6}$ for the γ-part. The model was applied for Os-180, Dy-162, Gd-160, Ru-100, Pd-114, and Xe-124 nuclei. According to the results, the outcomes of the fit shows good agreement with the experimental data, which arisen from adding two free parameters, V_0 and q, to Hulthen potential to control the depth of potential and shaped deformation. Then, numerical calculations for the excited energy and $B(E2)$ transition rates of proposed models were calculated and compared with the experimental data. This model by the rigidity parameter χ enables a better description of energy spectra for both of the phase transition from spherical to axially deformed nuclei $(X(3)\cup X(5)-H)$ and from prolate to oblate shapes $(Z(3)\cup Z(5)-H)$.

References

Alimohammadi, M. and Hassanabadi, H. (2017). Investigation of the spectroscopy properties of deformed nuclei by combining the X(3) and E(5) models. *The European Physical Journal A*, 53(6):129.

Bijker, R., Casten, R., Zamfir, N., et al. (2003). Test of X(5) for the γ Degree of Freedom. *Physical Review C*, 68(6):064304.

Bonatsos, D., Lenis, D., Minkov, N., et al. (2004a). Ground state bands of the E(5) and X(5) critical symmetries obtained from Davidson potentials through a variational procedure. *Physics Letters B*, 584(1-2):40–47.

Bonatsos, D., Lenis, D., Petrellis, D., et al. (2004b). Z(5): critical point symmetry for the prolate to oblate nuclear shape phase transition. *Physics Letters B*, 588(3-4):172–179.

Bonatsos, D., Lenis, D., Petrellis, D., et al. (2006). X(3): an exactly separable γ-rigid version of the X(5) critical point symmetry. *Physics Letters B*, 632(2-3):238–242.

Bonatsos, D., Lenis, D., Petrellis, D., et al. (2007a). Critical point symmetries in nuclei. *Bulg. J. Phys*, 34:227–239.

Bonatsos, D., McCutchan, E., Minkov, N., Casten, R., Yotov, P., Lenis, D., Petrellis, D., and Yigitoglu, I. (2007b). Exactly separable version of the Bohr Hamiltonian with the Davidson potential. *Physical Review C*, 76(6):064312.

Budaca, R. (2014a). Harmonic oscillator potential with a sextic anharmonicity in the prolate γ-rigid collective geometrical model. *Physics Letters B*, 739:56–61.

Budaca, R. (2014b). Quartic oscillator potential in the γ-rigid regime of the collective geometrical model. *The European Physical Journal A*, 50(5):87.

Budaca, R. and Budaca, A. (2015a). Competing γ-rigid and γ-stable vibrations in neutron-rich Gd and Dy isotopes. *The European Physical Journal A*, 51(10):126.

Budaca, R. and Budaca, A. (2015b). Conjunction of γ-rigid and γ-stable collective motions in the critical point of the phase transition from spherical to deformed nuclear shapes. *Journal of Physics G: Nuclear and Particle Physics*, 42(8):085103.

Budaca, R. and Budaca, A. (2016). Emergence of Euclidean dynamical symmetry as a consequence of shape phase mixing. *Physics Letters B*, 759:349–353.

Chabab, M., El Batoul, A., Hamzavi, M., et al. (2017). Excited collective states of nuclei within Bohr Hamiltonian with Tietz-Hua potential. *The European Physical Journal A*, 53(7):157.

Chabab, M., El Batoul, A., Lahbas, A., and Oulne, M. (2016). Electric quadrupole transitions of the Bohr Hamiltonian with Manning–Rosen potential. *Nuclear Physics A*, 953:158–175.

Chabab, M., Lahbas, A., and Oulne, M. (2015a). Bohr Hamiltonian with Hulthén plus ring-shaped potential for triaxial nuclei. *The European Physical Journal A*, 51(10):131.

Chabab, M., Lahbas, A., and Oulne, M. (2015b). Closed analytical solutions of Bohr Hamiltonian with Manning-Rosen potential model. *International Journal of Modern Physics E*, 24(11):1550089.

Edmonds, A. R. (1996). *Angular momentum in quantum mechanics*. Princeton university press.

Eshghi, M. and Hamzavi, M. (2012). Spin symmetry in Dirac-attractive radial problem and tensor potential. *Communications in Theoretical Physics*, 57(3):355.

Fortunato, L. (2004). Soft triaxial rotovibrational motion in the vicinity of $\gamma = \pi/6$. *Physical Review C*, 70(1):011302.

Greiner, W. and Maruhn, J. A. (1996). *Nuclear models*. Springer.

Hassanabadi, H. and Alimohammadi, M. (2018). Investigation of the Morse potential for the hybrid model and the one combining the E(5) and X(3) symmetries. *International Journal of Modern Physics E*, 27(06):1850053.

Hulthén, L. (1942a). Uber die Eigenlösungen der Schrödinger chung des Deutrons. *Arkiv för Matematik, Astronomi och Fysik*, 28(5).

Hulthén, L. (1942b). *Über die Eigenlösungen der Schrödinger-Gleichung des Deuterons*. Almqvist & Wiksell.

Iachello, F. (2000). Dynamic symmetries at the critical point. *Physical Review Letters*, 85(17):3580.

Iachello, F. (2001a). Analytic description of critical point nuclei in a spherical-axially deformed shape phase transition. *Physical Review Letters*, 87(5):052502.

Iachello, F. (2001b). Analytic description of critical point nuclei in a spherical-axially deformed shape phase transition. *Physical Review Letters*, 87(5):052502.

Ikhdair, S. M. (2009). Rotational and vibrational diatomic molecule in the Klein–Gordon equation with hyperbolic scalar and vector potentials. *International Journal of Modern Physics C*, 20(10):1563–1582.

Nikiforov, A. F. and Uvarov, V. B. (1988). *Special functions of Mathematical Physics*, volume 205. Springer.

Soheibi, N., Hamzavi, M., Eshghi, M., et al. (2017). Calculations of the decay transitions of the modified Pöschl–Teller potential model via Bohr Hamiltonian technique. *International Journal of Modern Physics E*, 26(11):1750073.